Electronic Supplementary Information (ESI) for *Chem. Commun.*

Degradation of Human Hemoglobin by Organic *C*-Nitroso Compounds

Jun Yi,* Guan Ye, Thomas M. Leonard and George B. Richter-Addo*

Department of Chemistry and Biochemistry, University of Oklahoma, 101 Stephenson Parkway, Norman, OK 73019, USA.

yijun@ou.edu; grichteraddo@ou.edu

Materials and Methods

Preparation of the Hb(RNO) (R = Me, Et) Derivatives: MetHb was prepared by oxidizing oxyHb with ferricyanide, and then dialyzing the protein against 20 mM sodium phosphate buffer at pH 6.8 to remove excess ferricyanide. The purified metHb was stored at –80 °C until needed. Solid sodium dithionite (100-150 mg) and the respective nitroalkane RNO_2 (50 μL; R = Me or Et) were added into the metHb solution (12 mL @ 40 mg/mL) and the mixture allowed to stand at 4 °C for 1 hour. The protein mixture was centrifuged and the precipitant discarded.

Cystallization: Crystals of the Hb(RNO) derivatives were obtained using the batch method according to published procedures for Hb derivatives.[1] Several pH conditions in the 5.6–7.0 range were achieved by varying the volume ratios of sodium phosphate (monobasic; 3.2 M) to potassium phosphate (dibasic; 3.2 M). 100 μL of protein solutions (40 mg/mL) were added into various amounts (0.18–0.38 mL) of phosphate buffer as well as 1–2 drops of toluene in 3 mL-sized vacutainer tubes. The protein solutions were mixed gently by slowly inverting the stoppered vacutainer tubes. Diamond shaped crystals of the Hb(RNO) (R = Me, Et) products started forming after ~3 days. Suitably sized Hb(RNO) crystals were harvested using cryo-loops, soaked in the mother liquor containing 16% glycerol for 5 min, and then flash-frozen in liquid nitrogen prior to data collection.

Choice of metHb vs oxyHb for reactions/crystallization: Using either metHb or oxyHb for the reaction with RNO_2/dithionite gave the same Hb(RNO) product UV-vis spectrum as shown in manuscript Fig. 1. However, crystals grown from the oxyHb reaction were not suitable for X-ray diffraction studies, whereas those grown from the metHb reaction were, as shown in Fig. S1 below.

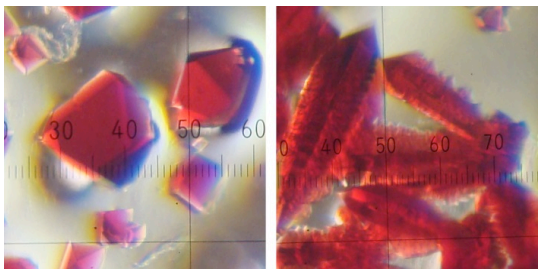

Fig. S1. Hb(EtNO) crystals grown from (left) the metHb/nitroethane/dithionite reaction, and (right) from the oxyHb/nitroethane/dithionite reaction.

X-ray diffraction data collection and processing

X-ray data were collected at 100 K on a RigakuMSC RU-H3R X-ray generator operated at 50 kV/100 mA to produce Cu/Kα radiation (λ = 1.5418 Å) at home source. For the Hb(MeNO) structure, 0.5° oscillation images were collected over a range of 100° with an exposure time of 5 min/image and a crystal-to-detector distance of 160 mm. For the Hb(EtNO) structure, 0.5° oscillation images were collected over a range of 145° with an exposure time of 5 min/image and a crystal-to-detector distance of 160 mm. Diffraction data were indexed and processed with the d*TREK program (Macintosh v.99D).[2]

Structure solution and refinement

In general, the phase information was obtained using the molecular replacement method as implemented in *PHASER* (v1.3.3).[3] The search model was the 1.8 Å resolution structure of human Hb nitrite (PDB access code 3D7O)[4] with all solvent molecules and nitrite ligands

removed. For the R_{free} calculation, 5% of randomly selected reflections were flagged and carried throughout the complete refinement procedure. The *CCP4* program *REFMAC* [5] and the *PHENIX* [6] refinement program were utilized for structure refinement. Bulk-solvent modeling and isotropic scaling of the observed and calculated structural amplitudes were used during the restrained refinements. *COOT* [7] was used for visualization and model building/corrections between refinement cycles. Water molecules were added to the structures using the "*Update Waters*" command in *PHENIX* at the later steps of refinements.

Hb(MeNO): The initial electron density map after molecular replacement revealed the presence of V-shaped Fe-bound ligands in the sixth positions for both alpha and beta subunits. The MeNO ligands were modeled into these V-shaped electron densities with the central N atom bound to Fe in both heme active sites. The nitrosomethane ligand file was imported from the monomer library implemented in the CCP4 suite with a molecular code of NSM. The Fe–N(nitrosomethane) bond distance and angle parameters were unrestrained throughout refinements; however, internal restraints of 1.22(2) Å (for *d*(N–O)), 1.45(2) Å (for *d*(C–N)) and 120(3)° (for ∠CNO) were applied to the nitrosomethane group. In addition to the axial ligands, three glycerol molecules were modeled into the crystal lattice based on the electron density map. The C-terminus residue of Arg141 in the alpha subunit was omitted from the structural model due to the poor electron density. The final crystallographic *R* and R_{free} (for the final model) of the human Hb(MeNO) structure are 0.224 and 0.28, respectively, in the 21.43–2.05 Å range.

Hb(EtNO): The initial electron density map revealed an axial ligand bound to heme Fe in the alpha distal pocket. The nitrosoethane ligand was modeled into this electron density map via the N atom bound to heme Fe. The crystallographic information file of nitrosoethane ligand was imported from the monomer library implemented in the CCP4 suite with a molecular code of NOE. The Fe–N(nitrosoethane) bond distance and angle parameters were unrestrained throughout refinements; however, internal restraints of 1.22(2) Å (for *d*(N–O)), 1.45(2) Å (for *d*(C2–N)) and 120(3)° (for ∠C2NO) were applied to the nitrosoethane group. One glycerol molecule was modeled in the crystal lattice located at the interface of two subunits.

The electron density map of the beta heme moiety was not as clear as that in the alpha subunit. In additional to the expected heme position, there was new electron density beneath the distal His63 sidechain that showed a weak interaction with the Nε atom of this residue. To evaluate the likelihood that the new density was due to a subpopulation of heme Fe, the *SFTool* and *FFT* programs in *CCP4* were used to calculate the Fe anomalous signals for this structure. In the anomalous map, there were two positive electron densities with an intensity ratio of 1:1, thus confirming that these signals were both from Fe in two positions (Fe_1 for the "original" heme site, and Fe_2 for the shifted heme that was ~5.0 Å shifted from its original position). The original heme was removed from the structural model to recalculate an unbiased difference electron density map for the beta heme site. Two heme molecules were modeled into the difference density map with 50% occupancy for each molecule guided by the iron anomalous map as well. There was no defined electron density showing axial ligand binding due to EtNO in the beta subunit.

The C-terminus residue of Arg141 in the alpha subunit was omitted from the structural model due to the lack of electron density. The final crystallographic *R* and R_{free} (for the final model) of the human Hb(EtNO) structure are 0.229 and 0.27, respectively, in the 21.4–2.0 Å range.

The $2F_o–F_c$ electron density maps and the $F_o–F_c$ electron density maps were generated using *FFT* as implemented in *CCP4*. The figures of electron density maps and the final model of the heme site of the human Hb(RNO) structures were drawn using PyMOL (Delano Scientific, 2006; http://www.pymol.org) and labels were added using Adobe® Photoshop.

Table S1. X-ray data collection and refinement statistics[a]

	Hb(MeNO)	Hb(EtNO)
Data Collection		
PDB accession code	4M4A	4M4B
Space group	$P4_12_12$	$P4_12_12$
Unit cell dimensions (Å)	53.57, 53.57, 191.87	53.44, 53.44, 193.58
Resolution range (Å)	21.43-2.05	21.4-2.0
Number of observations	110487	203574
Unique reflections	18023	19790
Average multiplicity	6.13(6.44)	10.29(7.05)
Completeness (%)	97.7(92.9)	99.4(93.5)
$\langle I/\sigma(I)\rangle$	9.2(4.8)	22.1(5.8)
R_{merge}[b]	0.087(0.23)	0.044(0.274)
Refinement		
Number of protein atoms	2266	2180
Number of heteroatoms	168	218
R-factor[c]	0.224	0.229
R_{free}[d]	0.28	0.270
Average B-factor (Å^2)[e]	33.68	53.86
rms deviations[f]		
bond lengths (Å)	0.01	0.01
bond angles (^{o})	1.1	1.23
Ramachandran plot (%)[g]		
favored	97.9	97.52
outliers	0	0
rotamer outliers	0	0.87

[a] The data in brackets refer to the highest resolution shell.
[b] $R_{merge} = \Sigma_{hkl}\Sigma_i |I_i(hkl) - \langle I(hkl)\rangle|/\Sigma_{hkl}\Sigma_i I_i(hkl)$, where $I_i(hkl)$ is the ith used observation for unique hkl, and $\langle I(hkl)\rangle$ is the mean intensity for unique hkl.
[c] $R = \Sigma_{hkl}||F_{obs}| - |F_{calc}||/\Sigma_{hkl}|F_{obs}|$, where F_{obs} and F_{calc} are the observed and calculated structure factors, respectively.
[d] R_{free} was calculated using 5% of the randomly selected diffraction data which were excluded from the refinement.
[e] The average for the polypeptide atoms.
[f] deviations from ideal values.[8]
[g] calculated using *MolProbity* [9] as implemented in *PHENIX*.

The quaternary structures of the Hb(RNO) complexes: *For an authoritative discussion on quaternary R vs T structures, please see for example a recent review article.*[10]

We have compared our human Hb(RNO) crystal structures with representative quaternary T, R, R2 and R3 human Hb structures in terms of the root mean square deviation (rmsd) between the tetramers, as well as the critical contacts at the α1β2 interface that help define the description

of the quaternary state. The rmsd between the different structures with least-square superposition of Cα of the tetramers (Table S1) suggest that the Hb(RNO) structures assume the quaternary R conformation. Consistently, the α1β2 interface, also a measure of quaternary matrix,[10] of the Hb(RNO) structures is similar to that of the R state structures but different from the T, R2 or R3 structures (Fig. S2).

In typical R state structures, the α1β2 dimer interface residue β2His97 lies between residues α1Thr41 and α1thr38, which is what we observe in our ordered Hb(MeNO), although it lacked the R state H-bond interaction between the carbonyl atom of β2His97 and the hydroxyl of α1Thr38 (Fig. S2). In the quaternary T state structure, the α1β2 dimer interface rearranges, resulting in β2His97 jumping a turn to locate between α1Pro44 and α1Thr41, while in the R2 structure the rearrangement of the α1β2 has moved β2His97 significantly away from both α1Thr41 and α1Thr38, although it is still located between these two residues.

Table S2. RMSD calculations[a]

	PDB i.d.	description	rmsd XYZ (Å)	ref.
Hb(EtNO)	4M4B (magenta)	*this work*	0.364	-
Hb(CO)	1AJ9 (red)	R state	0.475	[11]
deoxyHb[b]	1B86 (blue)	T state	2.544	[12]
Hb(CO)	1BBB (black)	R2 state	1.681	[13]
Hb(CO)	1YZI (cyan)	R3 state	1.72	[14]

[a] For this calculation, we fixed the Cα chains of the reference tetrameric Hb(MeNO) structure, and performed the rms deviations for Cα chains of the other tetrameric structures. [b] In complex with 2,3-DPG.

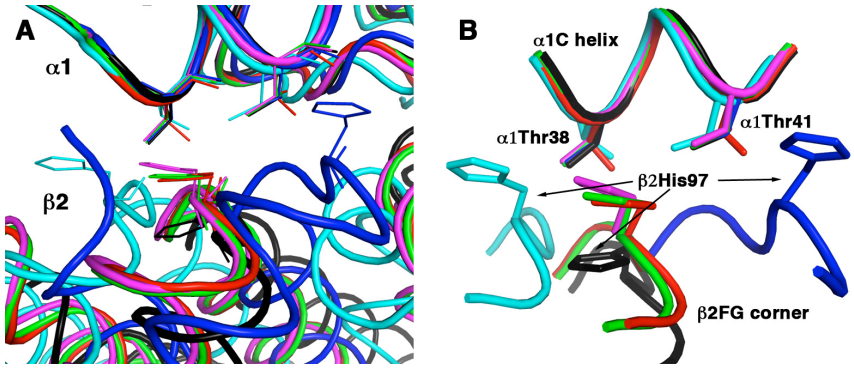

Fig. S2. The α1β2 interface of representative Hb structures. (**A**) The α1β1 subunits were superimposed using a T state deoxy Hb structure as the reference (PDB accession code: 1B86, 2.5 Å resolution; shown in blue).[12] This generates the same positions of the α1 C helices, but clearly shows different positions of the β2 FG corners for different quaternary structures. The R state Hb(CO) (PDB accession code: 1AJ9, 2.2 Å resolution)[11] is shown in red; the R2 state Hb(CO) (PDB accession code: 1BBB, 1.7 Å resolution)[13] is shown in black; and the R3 state Hb(CO) (PDB accession code: 1YZI, 2.07 Å resolution)[14] is shown in cyan; the Hb(MeNO) (PDB accession code: 4M4A, 2.05 Å resolution; this work) is shown in green; the Hb(EtNO) (PDB accession code: 4M4B, 2.0 Å resolution; this work) is shown in magenta. (**B**) Highlights of key residues (α1Thr38, α1Thr41 and β2His97) at this α1β2 interface. This analysis shows that the Hb(RNO) structures are in the R state.

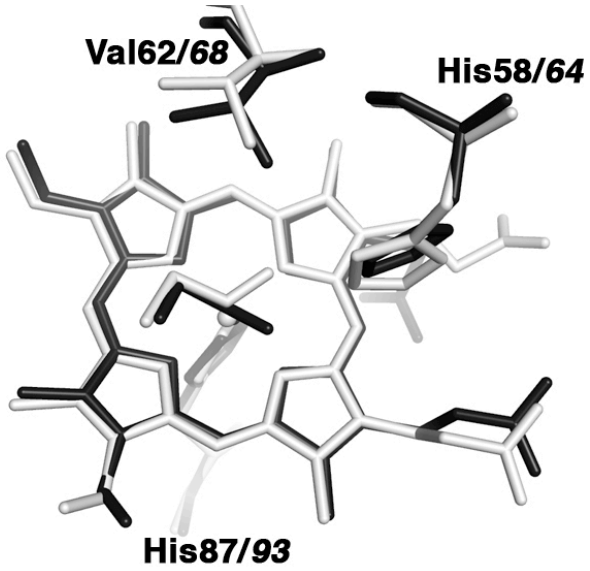

Fig. S3. Overlay of the heme active sites of the alpha subunit of Hb(EtNO) (light grey) and that of Mb(EtNO) (black), showing the relative orientations of the EtNO ligands. The residue numbers in italics are for Mb(EtNO).

References

1. M. K. Safo and D. J. Abraham, *Methods Mol. Med.* 2003, **82**, 1-19.
2. J. Pflugrath, *Acta Cryst.* 1999, **D55**, 1718-1725.
3. A. J. McCoy, R. W. Grosse-Kunstleve, P. D. Adams, M. D. Winn, L. C. Storoni and R. J. Read, *J. Appl. Cryst.* 2007, **40**, 658-674.
4. J. Yi, M. K. Safo and G. B. Richter-Addo, *Biochemistry* 2008, **47**, 8247-8249.
5. G. N. Murshudov, A. A. Vagin and E. J. Dodson, *Acta Cryst.* 1997, **D53**, 240-255.
6. P. D. Adams, P. V. Afonine, G. Bunkoczi, V. B. Chen, I. W. Davis, N. Echols, J. J. Headd, L. W. Hung, G. J. Kapral, R. W. Grosse-Kunstleve, A. J. McCoy, N. W. Moriarty, R. Oeffner, R. J. Read, D. C. Richardson, J. S. Richardson, T. C. Terwilliger and P. H. Zwart, *Acta Cryst.* 2010, **D66**, 213-221.
7. P. Emsley, B. Lohkamp, W. G. Scott and K. Cowtan, *Acta Cryst.* 2010, **D66**, 486-501.
8. R. A. Engh and R. Huber, *Acta Cryst.* 1991, **A47**, 392-400.
9. V. B. Chen, W. B. Arendall, J. J. Headd, D. A. Keedy, R. M. Immormino, G. J. Kapral, L. W. Murray, J. S. Richardson and D. C. Richardson, *Acta Cryst.* 2010, **D66**, 12-21.
10. M. K. Safo, M. H. Ahmed, M. S. Ghatge and T. Boyiri, *Biochim. Biophys. Acta* 2011, **1814**, 797-809.
11. G. B. Vasquez, X. Ji, C. Fronticelli and G. L. Gilliland, *Acta Cryst.* 1998, **D54**, 355-366.
12. V. Richard, G. G. Dodson and Y. Mauguen, *J. Mol. Biol.* 1993, **233**, 270-274.
13. M. M. Silva, P. H. Rogers and A. Arnone, *J. Biol. Chem.* 1992, **267**, 17248-17256.
14. M. K. Safo and D. J. Abraham, *Biochemistry* 2005, **44**, 8347-8359.